Journal of Materials Chemistry B

ROYAL SOCIETY OF CHEMISTRY

COMMUNICATION

View Article Online
View Journal | View Issue

Cite this: J. Mater. Chem. B, 2021, 9, 5451

Received 19th May 2021,
Accepted 20th June 2021

DOI: 10.1039/d1tb01126j

rsc.li/materials-b

A robust CRISPR–Cas12a biosensor coated with metal–organic framework†

Lingjun Sha,[a] Yiwei Han,[b] Minghui Wang,[b] Shuai Wu,*[b] Jie Yang[b] and Genxi Li *[ab]

Metal–organic frameworks (MOFs) are proposed to protect a CRISPR-associated enzyme/RNA complex from harsh environments, while the complex can be quickly released from MOFs with high efficiency. Therefore, the application of CRISPR-powered biosensing can be more feasible.

The clustered regularly interspaced short palindromic repeats (CRISPR) and CRISPR-associated (CRISPR–Cas) immune systems have recently been utilized in biosensing applications.[1] These emerging approaches allow rapid and cost-efficient detection of various targets with high sensitivity and specificity, thereby making them powerful diagnostic tools for point-of-care (POC) testing, such as SHERLOCK (specific high sensitivity enzymatic reporter unlocking), DETECTOR (DNA endonuclease-targeted CRISPR trans reporter), and Cas14-DETECTR.[2–4] In particular, CRISPR-based COVID-19 diagnostics has shown great clinical application potential.[5,6] In general, these CRISPR-mediated biosensing strategies are highly dependent on the collateral cleavage activities of RNA-guided Cas proteins towards the single-stranded DNA (ssDNA) or RNA.[7] However, as with most proteins, Cas proteins (such as Cas13a, Cas12a, or Cas14) are susceptible to external interference including elevated temperature, most organic reagents, and inhibitors.[8] Thus, the relevant diagnostic reagents are generally required to be maintained under strictly controlled conditions. For instance, a cold chain system has to be established for the purpose of transportation and storage. Nevertheless, the system is not always feasible in resource-poor settings, such as deprived areas or disaster areas, and it also imposes a huge economic and environmental burden.[9] Therefore, it is imperative to develop low-cost approaches to preserve their biological activities, which can further boost the practical applications of CRISPR-powered biosensing.

Metal–organic frameworks (MOFs) are three-dimensional crystalline nanoporous materials constructed by joining metal-based nodes with organic linkers.[10–12] Compared with conventional inorganic porous materials, the modular approach to synthesize MOFs offers many advantages such as high surface area, tunable porosity, and their highly unusual flexibility, which has allowed MOFs to be candidate materials for gas separation,[13] catalysis,[14–16] electric conduction,[17–21] sensing,[22,23] and more biomedical applications.[24,25] More importantly, the degradation of porous MOF exoskeletons can be controlled by simply modulating different ambient conditions, such as pH, which drives them closer toward drug delivery and biological conservation.[26,27] For instance, the cytosolic delivery of CRISPR/Cas9 for efficient genome editing using MOFs has been reported by Khashab's group.[28,29] Therefore, we hypothesize that MOFs can be a class of propitious materials to preserve the biological activities of CRISPR-associated enzyme/RNA complexes for biosensing.

In this study, the CRISPR–Cas12a system mediated by Cas12a protein with collateral cleavage activity has been chosen as a model, allowing the degradation of any nonspecific ssDNA near the target DNA.[30] As shown in Scheme 1, Cas12a protein is firstly incubated with its own guide CRISPR RNA (crRNA) to form the Cas12a/crRNA complex. Then, zeolitic imidazolate frameworks-8 (ZIF-8), a subclass of MOFs, are introduced as they possess high thermal and chemical stability.[31] Herein, the self-assembly of 2-methylimidazole (2-MIM) and Zn^{2+} with the complex forms Cas12a/crRNA@ZIF-8 nanocomposites, and thus Cas12a/crRNA is encapsulated with high efficiency. The whole process is carried out under mild conditions, and the reaction time is very short. Moreover, it has been demonstrated that ZIF-8 encapsulation can preserve Cas12a/crRNA against high temperature, proteolysis, and organic solvents. More importantly, the incorporated complex can be released under mild conditions. So, the crRNA-complementary activator ssDNA can be targeted to activate the collateral cleavage activity toward fluorophore

[a] Center for Molecular Recognition and Biosensing, School of Life Sciences, Shanghai University, Shanghai 200444, P. R. China. E-mail: genxili@nju.edu.cn
[b] State Key Laboratory of Pharmaceutical Biotechnology, School of Life Sciences, Nanjing University, Nanjing 210023, P. R. China. E-mail: shwu@njmu.edu.cn

† Electronic supplementary information (ESI) available. See DOI: 10.1039/d1tb01126j

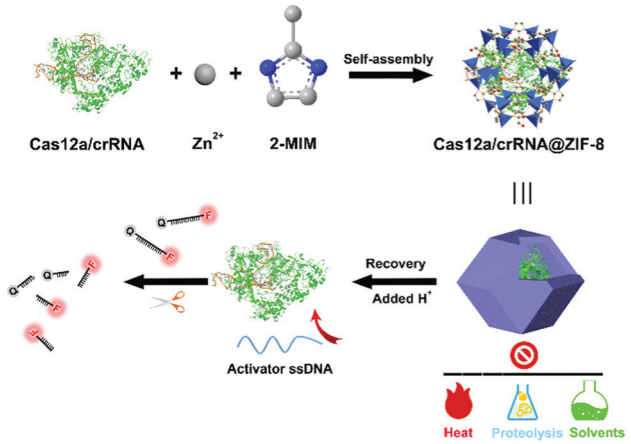

Scheme 1 Schematic representation of the coating strategy for the Cas12a/crRNA complex and its application for detecting nucleic acids.

quencher-labeled reporter ssDNA by the Cas12a/crRNA complex, thereby realizing signal amplification. By evaluating the detection performance of Cas12a/crRNA recovered from the ZIF-8 shell, we have demonstrated that the CRISPR–Cas12a sensor protected by MOFs has very high stability and sensitivity.

To construct the CRISPR–Cas12a biosensor, as shown in Fig. 1A, a crRNA with stem-loop structure, the 3′-end of which is partially complementary with activator ssDNA, has been designed to bind to the Cas12a protein. After the formation of the Cas12a/crRNA complex, the target binding to the crRNA will unleash the enzyme activity. In this circumstance, the short strands of ssDNA reporters labeled with a fluorophore (carboxyfluorescein, FAM) and quencher (black hole quencher, BHQ) pair at the two ends can be degraded, leading to the separation of the fluorophore and thus generating an appreciable fluorescent signal. Then, we have employed different analytes to verify the feasibility of this sensor. As shown in Fig. 1B, activator ssDNA shows a significantly strong fluorescent signal, compared to the result in the absence of the targets. Besides, it can be seen that the random ssDNA also gives a negligible signal response. These results have shown that only target-DNA binding can activate the cleavage activity of Cas12a/crRNA, demonstrating the feasibility of the CRISPR–Cas12a sensor.

Then, we employed MOFs to protect the CRISPR–Cas12a biosensor; Cas12a/crRNA@ZIF-8 was prepared by mixing the Cas12a/crRNA complex and 2-methylimidazole solution, followed by the addition of zinc nitrate solution at room temperature under mechanical agitation. The resulting products are then collected by centrifugation and washed with deionized water three times to remove excess residues. Scanning electron microscopy (SEM) and transmission electron microscopy (TEM) images reveal that Cas12a/crRNA@ZIF-8 grew into monodisperse nanostructures with a particle diameter of 400–600 nm (Fig. 2A and B). The images at high magnifications show more details of the material morphology. As shown in Fig. S1A and B (ESI†), the nanocomposite presents an irregular rhombic dodecahedron with a slightly uneven surface, compared to pure ZIF-8 nanoparticles (Fig. S2, ESI†), which may be caused by the embedding of biomolecules. The crystal phase of the as-synthesized materials is further confirmed using the powder X-ray diffraction (PXRD) technique. As illustrated in Fig. 2C, the patterns of Cas12a/crRNA@ZIF-8, the actual ZIF-8, and that of the simulated ZIF-8 are very similar, suggesting that the ZIF-8 crystal structure is well maintained in the CIRSPR-loaded nanoparticles. Additionally, zeta potential measurements indicate the formation of nanocomposites. As shown in Fig. 2D, the positively charged Cas12a (+15.2 mV) becomes negatively charged upon the binding of crRNA (−29.8 mV). After the self-assembly process between Cas12a/crRNA and the ZIF-8 precursors, the potential is measured at +8.2 mV. Meanwhile, the characteristic absorption bands at 1675 cm^{-1} recorded using Fourier transform infrared

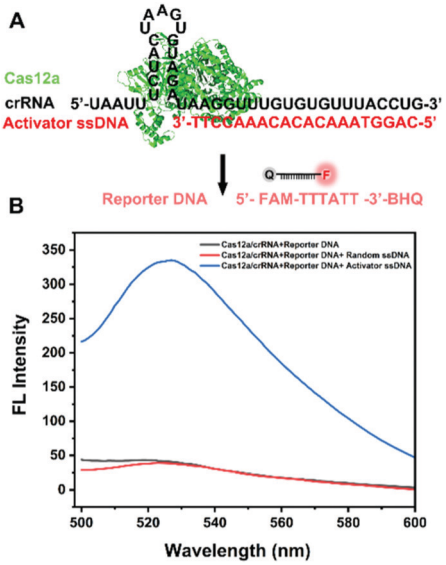

Fig. 1 (A) Design of the crRNA, Activator ssDNA, and Reporter ssDNA. (B) Fluorescent spectra of the detection of target Activator ssDNA, Random-ssDNA, and no targets *via* the CRISPR–Cas12a sensor.

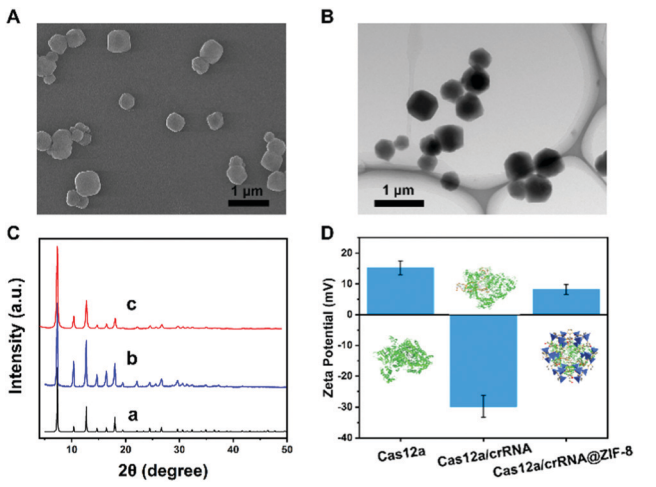

Fig. 2 (A) SEM and (B) TEM micrographs of Cas12a/crRNA@ZIF-8. (C) PXRD of simulated ZIF-8 (a), actual ZIF-8 (b), and Cas12a/crRNA@ZIF-8 (c). (D) Zeta-potential of free Cas12a, Cas12a/crRNA complex, and Cas12a/crRNA@ZIF-8. Error bars are derived from three parallel experiments.

spectroscopy (FT-IR) (Fig. S3, ESI†) and the reduction of the BET area (Fig. S4, ESI†) confirm the presence of the Cas12a/crRNA complex. Collectively, the above results indicate that the nanocomposite has been successfully prepared.

Cas12a/crRNA loading efficiency and pH responsive release have been evaluated by measuring the change of ultraviolet (UV) absorbance value at 260 nm. As shown in Fig. S5A (ESI†), the free Cas12a/crRNA solution shows a high absorbance value at 260 nm, but after assembly with ZIF-8, the absorbance value of the supernatant decreases significantly, indicating that the Cas12a/crRNA complex will enter into the nanostructure of ZIF-8. According to the established standard curve (Fig. S5B, ESI†), the wrapping efficiency of Cas12a/crRNA can be calculated. Under the optimized conditions (Table S1, ESI†), the maximum is 87%, showing a high loading capacity. To further investigate the effect of pH on the release process, we have monitored the UV spectrum of Cas12a/crRNA@ZIF-8 in the phosphate-buffered saline (PBS) solution under physiological (pH 7.4) and acidic (pH 4–6) conditions. As shown in Fig. 3A, there is virtually no release of Cas12a/crRNA complex from the nanocomposite under physiological conditions. However, 98%, 91%, 80%, and 65% of complexes are released in 10 min at pH 4, 5, 5.5, and 6, respectively. The maximum release of Cas12a/crRNA complex is achieved at pH 4, 5 and 5.5, indicating that acidic conditions can effectively destroy the structure of ZIF-8. Additionally, the released complex (M_W: ~138 kDa) can be purified using ultrafiltration with 100 kDa molecular weight cut off (MWCO) devices. We have fabricated CRISPR–Cas12a sensors by using the recovered complex under different pH and the original complex to compare the detection performance. As shown in Fig. 3B, the difference in the two linear curves (Free Cas12a/crRNA and released complex under pH 5.5) is very small, which demonstrates that this recovered Cas12a/crRNA still has high biological activity. However, the detection performance of the recovered complex under pH 6 is reduced, which may be because it cannot be completely released from the material. Meanwhile, it should be noted that the low pH solution (pH 4 and 5) may affect the enzyme activity. Thus, pH 5.5 is selected for the following steps.

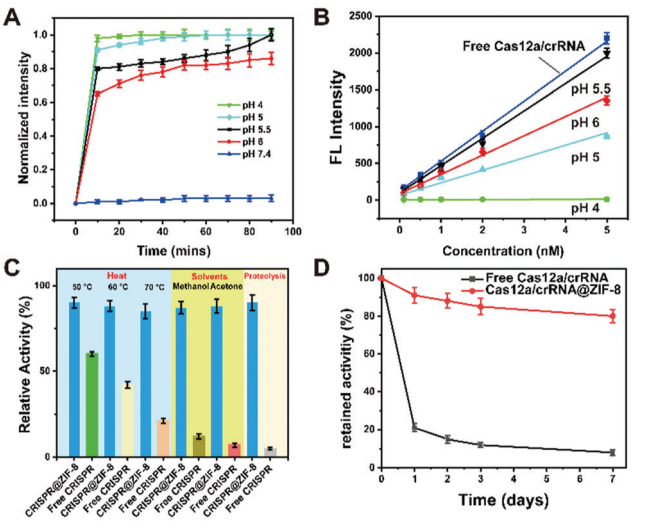

Fig. 3 (A) pH dependent release of Cas12a/crRNA complex from MOFs under physiological (pH 7.4) and acidic (pH 4–6) conditions. (B) Comparison of sensor performance using the released Cas12a/crRNA complex under different pH values. (C) Relative activity of free CRISPR and CRISPR@ZIF-8 under different interference conditions. Data are normalized against free Cas12a/crRNA activity at room temperature. (D) Protective performance of MOFs for Cas12a/crRNA in the long-term storage test. Error bars are derived from three parallel experiments.

In order to study the protective effect of MOF on the CRISPR–Cas12a sensor, Cas12a/crRNA with and without ZIF-8 coating has been treated with a series of external interference conditions, including high-temperature, organic reagents, and proteolytic enzymes, which would knock the proteins out of commission. We have first measured the bioactivity of CRISPR@ZIF-8 and the free CRISPR system at 50, 60, and 70 °C and normalized the resulting data to "relative activity". This means the collateral cleavage activity of free Cas12a/crRNA and the released Cas12a/crRNA when targeting complementary ssDNA under the same conditions, which is relative to the original activity of free Cas12a/crRNA without any treatment. As shown in Fig. 3C, the detection performance of a free CRISPR-based sensor system is much weaker than that of CRISPR@ZIF-8 at the same temperature. Without shell protection *via* encapsulation, the activity of free Cas12a/crRNA decreases greatly with the elevated temperature. However, the MOF-coated detection system retains over 80% of bioactivity at 70 °C, showing a very high thermal stability. What's more, after exposure to organic solvents (methanol or acetone) for 1 h, as expected, most of the free CRISPR systems lose their biological function, while the systems recovered from CRISPR@ZIF-8 still maintain good detection performance, suggesting improved chemical resistance. Remarkably, in the presence of a proteolytic enzyme (protease K), the protected Cas12a/crRNA complex essentially retains bioactivity, however, the free CRISPR system can hardly detect targets. Additionally, to further investigate the ability of long-term storage, we have challenged the two biosensing systems at room temperature for a week. As shown in Fig. 3D, the system based on Cas12a/crRNA@ZIF-8 is able to maintain about 80% of its activity, while the activity of the free CRISPR system is basically lost the next day, which may be due to the RNA degradation. All the above results indicate that the CRISPR–Cas12a sensor constructed with MOF protection has very high stability, providing great application potentials for medical diagnosis.

To further prove the universality and practicability of this protected CRISPR–Cas12a sensor, we have also re-designed the nucleotide sequence of the CRISPR system so that it can be employed for a wider range of targets. Herein, mucin 1 (MUC1) protein, a well-known cancer biomarker, has been selected as a target, which is always overexpressed in various cancers such as breast, colorectal, lung, ovarian, and pancreatic cancer.[32,33] The schematic diagram is shown in Fig. 4A; a binding-DNA (B-DNA) containing the MUC1 aptamer sequence has been designed to hybridize with an activator-DNA (A-DNA) to form a stable double-stranded DNA (dsDNA). In the absence of MUC1, the DNA hybridization with a melting temperature above room temperature can effectively prevent the binding of B-DNA to

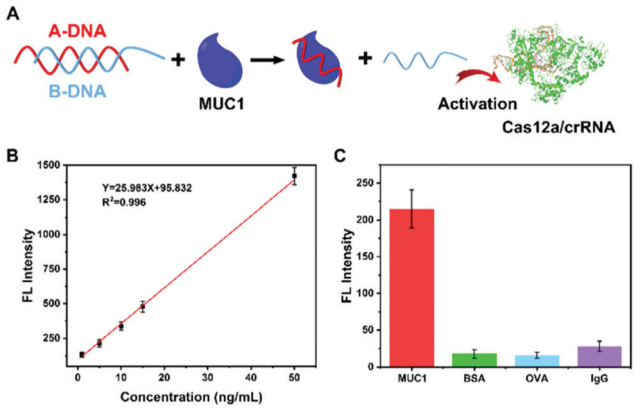

Fig. 4 (A) Schematic representation of the detection strategy for MUC1 using released Cas12a/crRNA. (B) Linear calibration curve of MUC1 detection. (C) Selectivity experiments through comparison of the fluorescence intensity in the presence of 5 ng mL^{-1} MUC1 and non-target proteins. Error bars were derived from three parallel experiments.

the Cas12a/crRNA complex, which is released from ZIF-8. On the other hand, once MUC1 is introduced, target binding to the B-DNA will competitively liberate the A-DNA from the duplex structure to activate the collateral cleavage activity of Cas12a/crRNA, thus cleaving the reporter ssDNA. The concentration of MUC1 can be determined by measuring the change of fluorescence intensity. As shown in Fig. 4B, a good linear relationship between the fluorescence intensity and the concentration of MUC1 can be obtained in the range from 1 ng to 50 ng mL^{-1}. The detection limit of MUC1 is 0.3 ng mL^{-1}. To further evaluate the specificity of the sensor, control experiments have been conducted. As shown in Fig. 4C, under the same experimental conditions, these signal readouts of other proteins, including bovine serum albumin (BSA), ovalbumin (OVA), and IgG, are largely close to that of the blank control. All these results manifest that this MOF-coated CRISPR system could be employed for detecting protein targets with good sensitivity and selectivity, which further promotes the application of CRISPR-powered biosensing for medical diagnosis.

In summary, we have demonstrated that MOFs can be employed as a protective coating to preserve the bioactivity of the Cas12a/crRNA complex to construct a robust sensor. With the protection of MOFs, the Cas12a/crRNA complex is able to withstand perturbation environments, such as elevated temperatures, organic solvents, and proteolytic agents, achieving stable and long-term storage. More importantly, the complex can be quickly and simply recovered from the formed nanocomposites, and meanwhile, retain their collateral cleavage activities to develop a robust CRISPR–Cas12a biosensor. Therefore, the MOF coating can greatly improve the stability of biological reagents and reduces the cost of cold chain transportation, and shows promising potential for POC diagnosis in resource-limited settings. The MOF-coated CRISPR-associated enzyme/RNA complex may also provide a new insight into the preparation of biological agents for biocatalysis, which shows great potential in disease diagnosis and treatment as well as environmental monitoring. Exploring the self-assembly behavior among different MOFs and CRISPR-associated enzyme/RNA to improve the bioactivity will further promote the application of gene editing technology *in vivo* and *in vitro*.

This work was supported by the National Natural Science Foundation of China (Grant No. 81772593).

Conflicts of interest

There are no conflicts to declare.

Notes and references

1 R. Bruch, G. A. Urban and C. Dincer, *Trends Biotechnol.*, 2019, **37**, 791–792.
2 J. S. Gootenberg, O. O. Abudayyeh, J. W. Lee, P. Essletzbichler, A. J. Dy, J. Joung, V. Verdine, N. Donghia, N. M. Daringer, C. A. Freije, C. Myhrvold, R. P. Bhattacharyya, J. Livny, A. Regev, E. V. Koonin, D. T. Hung, P. C. Sabeti, J. J. Collins and F. Zhang, *Science*, 2017, **356**, 438–442.
3 J. S. Chen, E. Ma, L. B. Harrington, M. Da Costa, X. Tian, J. M. Palefsky and J. A. Doudna, *Science*, 2018, **360**, 436–439.
4 L. B. Harrington, D. Burstein, J. S. Chen, D. Paez-Espino, E. Ma, I. P. Witte, J. C. Cofsky, N. C. Kyrpides, J. F. Banfield and J. A. Doudna, *Science*, 2018, **362**, 839–842.
5 J. P. Broughton, X. Deng, G. Yu, C. L. Fasching, V. Servellita, J. Singh, X. Miao, J. A. Streithorst, A. Granados, A. Sotomayor-Gonzalez, K. Zorn, A. Gopez, E. Hsu, W. Gu, S. Miller, C. Y. Pan, H. Guevara, D. A. Wadford, J. S. Chen and C. Y. Chiu, *Nat. Biotechnol.*, 2020, **38**, 870–874.
6 J. Joung, A. Ladha, M. Saito, N. G. Kim, A. E. Woolley, M. Segel, R. P. J. Barretto, A. Ranu, R. K. Macrae, G. Faure, E. I. Ioannidi, R. N. Krajeski, R. Bruneau, M. W. Huang, X. G. Yu, J. Z. Li, B. D. Walker, D. T. Hung, A. L. Greninger, K. R. Jerome, J. S. Gootenberg, O. O. Abudayyeh and F. Zhang, *N. Engl. J. Med.*, 2020, **383**, 1492–1494.
7 J. S. Gootenberg, O. O. Abudayyeh, M. J. Kellner, J. Joung, J. J. Collins and F. Zhang, *Science*, 2018, **360**, 439–444.
8 L. Zhang, Y. Li, Y. Ying and Y. Fu, *TrAC, Trends Anal. Chem.*, 2019, **118**, 434–443.
9 L. J. Wolfson, F. Gasse, S. P. Lee-Martin, P. Lydon, A. Magan, A. Tibouti, B. Johns, R. Hutubessy, P. Salama and J. M. Okwo-Bele, *Bull. W. H. O.*, 2008, **86**, 27–39.
10 H. Furukawa, K. E. Cordova, M. O'Keeffe and O. M. Yaghi, *Science*, 2013, **341**, 1230444.
11 S. Z. Wang, C. M. McGuirk, A. d'Aquino, J. A. Mason and C. A. Mirkin, *Adv. Mater.*, 2018, **30**, 1800202.
12 Y. Yuan, Y. Yang and G. Zhu, *EnergyChem*, 2020, **2**, 100037.
13 J. R. Li, R. J. Kuppler and H. C. Zhou, *Chem. Soc. Rev.*, 2009, **38**, 1477–1504.
14 J. Lee, O. K. Farha, J. Roberts, K. A. Scheidt, S. T. Nguyen and J. T. Hupp, *Chem. Soc. Rev.*, 2009, **38**, 1450–1459.
15 E. Asadian, S. Shahrokhian and A. Iraji Zad, *Int. J. Hydrogen Energy*, 2020, **45**, 1890–1900.
16 Y. Wang, Y. Wang, L. Zhang, C.-S. Liu and H. Pang, *Inorg. Chem. Front.*, 2019, **6**, 2514–2520.

17 C. Young, J. Kim, Y. V. Kaneti and Y. Yamauchi, *ACS Appl. Energy Mater.*, 2018, **1**, 2007–2015.
18 L. Wang, H. Liu, J. Zhao, X. Zhang, C. Zhang, G. Zhang, Q. Liu and H. Duan, *Chem. Eng. J.*, 2020, **382**, 122979.
19 W.-H. Li, W.-H. Deng, G.-E. Wang and G. Xu, *EnergyChem*, 2020, **2**, 100029.
20 G. Zhang, L. Jin, R. Zhang, Y. Bai, R. Zhu and H. Pang, *Coord. Chem. Rev.*, 2021, **439**, 213915.
21 Z. Wu, L. Wang, S. Chen, X. Zhu, Q. Deng, J. Wang, Z. Zeng and S. Deng, *Chem. Eng. J.*, 2021, **404**, 126579.
22 X. Zhu, H. Y. Zheng, X. F. Wei, Z. Y. Lin, L. H. Guo, B. Qiu and G. N. Chen, *Chem. Commun.*, 2013, **49**, 1276–1278.
23 G. Gumilar, Y. V. Kaneti, J. Henzie, S. Chatterjee, J. Na, B. Yuliarto, N. Nugraha, A. Patah, A. Bhaumik and Y. Yamauchi, *Chem. Sci.*, 2020, **11**, 3644–3655.
24 X. Liu, Z. Yan, Y. Zhang, Z. Liu, Y. Sun, J. Ren and X. Qu, *ACS Nano*, 2019, **13**, 5222–5230.
25 F. Wang, Y. Zhang, Z. Liu, Z. Du, L. Zhang, J. Ren and X. Qu, *Angew. Chem., Int. Ed.*, 2019, **58**, 6987–6992.
26 Y. Feng, H. Wang, S. Zhang, Y. Zhao, J. Gao, Y. Zheng, P. Zhao, Z. Zhang, M. J. Zaworotko, P. Cheng, S. Ma and Y. Chen, *Adv. Mater.*, 2019, **31**, e1805148.
27 C. Wang, S. Tadepalli, J. Luan, K. K. Liu, J. J. Morrissey, E. D. Kharasch, R. R. Naik and S. Singamaneni, *Adv. Mater.*, 2017, **29**, 1604433.
28 S. K. Alsaiari, S. Patil, M. Alyami, K. O. Alamoudi, F. A. Aleisa, J. S. Merzaban, M. Li and N. M. Khashab, *J. Am. Chem. Soc.*, 2018, **140**, 143–146.
29 M. Z. Alyami, S. K. Alsaiari, Y. Li, S. S. Qutub, F. A. Aleisa, R. Sougrat, J. S. Merzaban and N. M. Khashab, *J. Am. Chem. Soc.*, 2020, **142**, 1715–1720.
30 S. Y. Li, Q. X. Cheng, J. K. Liu, X. Q. Nie, G. P. Zhao and J. Wang, *Cell Res.*, 2018, **28**, 491–493.
31 K. S. Park, Z. Ni, A. P. Côté, J. Y. Choi, R. Huang, F. J. Uribe-Romo, H. K. Chae, M. O'Keeffe and O. M. Yaghi, *Proc. Natl. Acad. Sci. U. S. A.*, 2006, **103**, 10186–10191.
32 M. A. Hollingsworth and B. J. Swanson, *Nat. Rev. Cancer*, 2004, **4**, 45–60.
33 J. A. Ludwig and J. N. Weinstein, *Nat. Rev. Cancer*, 2005, **5**, 845–856.